Standard housing temperature but not β3-adrenoreceptor agonism drives weight-gain and adipose tissue deposition in rats following diet induced obesity at thermoneutrality

Peter Aldiss[1], Jo E Lewis[3], Irene Lupini[4], David Boocock[5], Amanda K Miles[5], Francis J P Ebling[3], Helen Budge[1] and Michael E Symonds[1, 2*].

[1] *The Early Life Research Unit, Division of Child Health, Obstetrics and Gynaecology, School of Medicine, University of Nottingham;* peter.aldiss@nottingham.ac.uk*; helen.budge@nottingham.ac.uk; michael.symonds@nottingham.ac.uk*

[2] *Nottingham Digestive Disease Centre and Biomedical Research Unit, School of Medicine, University of Nottingham*

[3] *School of Life Sciences, Queen's Medical Centre, University of Nottingham; fran.ebling@nottingham.ac.uk; jl2033@medschl.cam.ac.uk*

[4] *School of Biosciences and Veterinary Medicine, University of Camerino, Camerino, MC, Italy; Irene.lupini@studenti.unicam.it*

[5] *John van Geest Cancer Research Centre, Nottingham Trent University, Nottingham, NG11 8N; david.boocock@ntu.ac.uk; amanda.miles@ntu.ac.uk*

***** Correspondence: *michael.symonds@nottingham.ac.uk;* peter.aldiss@nottingham.ac.uk

Abstract

Background and aim: Rodents are commonly housed below thermoneutrality and this exposure to 'cold' (i.e. 20°C) activates thermogenic brown (BAT) and beiging of white adipose tissue. Here, we examined whether a standard housing temperature (i.e. 20°C, a reduction in temperature of ~8°C) or YM-178, a highly-selective β3-adrenoreceptor agonist, in obese animals raised at thermoneutrality, would impact differently on classical BAT or subcutaneous inguinal (IWAT) beige depots.

Methods: Eighteen weanling Sprague-Dawley rats were housed at thermoneutrality (28°C) and fed a high-fat diet. At 12 weeks, 6 animals were randomised to either standard housing temperature (20°C, n=6) or to β3-AR agonist administration (28°C+β3, 0.75mg/kg/d, n=6) for 4 weeks. Metabolic assessment was undertaken during the final 48h, followed by interscapular, perivascular BAT and IWAT sampling for the analysis of thermogenic genes and the proteome.

Results: Exposure to 20°C increased weight gain, BAT and IWAT mass. Proteomic analysis of BAT revealed novel pathways associated with cold-induced weight gain (i.e. histone deacetylation, glycosaminoglycan degradation and glycosphingolipid biosynthesis) whilst β3-adrenoreceptor agonism impacted on proteins involved in skeletal muscle contraction and cell differentiation. IWAT of cold-exposed animals exhibited an enrichment of proteins involved NAD+ binding, plus retinol and tyrosine metabolic pathways whilst β3-AR agonism downregulated ribosomal and upregulated acute phase response proteins.

Conclusion: Following diet-induced obesity at thermoneutrality, exposure to 20°C promotes subcutaneous fat deposition in order to reduce heat loss and defend body temperature. In contrast, chronic administration of β3-AR agonist has minimal metabolic-related effects on adipose tissue.

Introduction

Therapeutic activation of thermogenic brown adipose tissue (BAT) may be feasible to prevent, or treat, cardiometabolic disease [1]. In rodent models of obesity, the activation of BAT and UCP1-positive beige adipocytes in white adipose tissue (WAT) by cold exposure and sympathomimetics (i.e. β3-agonists) can attenuate or reverse obesity, diabetes and atherosclerosis, thus eliciting beneficial effects on metabolic health [1]. One factor which could influence these outcomes is that animals are typically housed at temperatures well below their thermoneutral zone (which for a rodent is c. 28°C) [2]. Under these conditions, not only is BAT active, but UCP1+ beige adipocytes are readily seen in the inguinal WAT (IWAT) depot which is considered 'beige'.

Housing animals at thermoneutrality modifies the thermogenic and metabolic response. For example, fasting glucose, food intake and metabolic rate are reduced at a higher ambient temperature [3]. Furthermore, markers of 'browning' and BAT activation are reduced at thermoneutrality, whilst the primary organ responsible for glucose uptake becomes skeletal muscle and not BAT [3]. Long term housing at thermoneutrality reduces sympathetic drive in BAT, as demonstrated by reduced tyrosine hydroxylase and norepinephrine turnover [4]. This results in increased adiposity at thermoneutrality, despite a lower energy intake compared to animals housed at 20°C. Thermoneutral housing also attenuates the response to common thermogenic stimuli. For instance, the thermogenic effects of thyroxine become independent of UCP1 due to the onset of pyrexia [5]. Similarly, the induction of 'browning' seen with exercise training at standard housing is attenuated in animals housed at thermoneutrality [6].

The 'cold-stressed' animal has been widely studied but much less is known about the underlying adaptations in adipose tissue in animals maintained at thermoneutrality. Usually, temperatures as low as 4°C, which represents an 'extreme cold', are used to activate BAT, with the induction of UCP1 and subsequent thermogenic response primarily seen in

subcutaneous IWAT and other 'beige' depots [7]. Conversely, when animals which have been housed at thermoneutrality and are then exposed to 20°C, the induction of UCP1 is primarily seen in BAT. These differences highlight that there are two key steps to the 'browning' process and emphasise the need to study metabolism under more translationally relevant conditions [7]. Importantly, it was recently demonstrated that BAT from thermoneutrally housed, obese animals closer resembles human BAT and, that this model of 'humanised BAT' represents the best choice for modelling BAT physiology [8]. Here, we aimed to determine the metabolic response to modest cold exposure (i.e. standard housing temperatures (20°C)), which constitutes a drop of c. 8°C and chronic β3-AR agonism in animals raised from weaning at thermoneutrality. Using this model, in which animals are not 'cold-stressed' and BAT is chronically inactive, we have demonstrated UCP1 mRNA is absent in subcutaneous IWAT (the classical 'beige' depot) and not induced with exercise training, a common response at standard housing temperatures [9]. We hypothesised that exposure to a mild cold stimulus in animals raised at thermoneutrality would have modest effects on systemic metabolism but not weight per se. Instead, we demonstrate rapid weight gain in response to an 8°C reduction in ambient temperature and deposition of substantial amounts (125%) of subcutaneous adipose tissue through an, as yet, unexplained mechanism. These effects were not seen in animals treated with the highly-selective β3-adrenoreceptor agonist, YM-178, suggesting a direct effect of ambient temperature which is uncoupled from sympathetic activation. Using adipose tissue proteomics, we then uncovered novel pathways associated with this cold-induced weight gain illustrating a potentially novel mechanism through which animals defend body temperature in the absence of a thermogenic response.

Methods

Animals, cold exposure and YM-178 treatment

All studies were approved by the University of Nottingham Animal Welfare and Ethical Review Board, and were carried out in accordance with the UK Animals (Scientific Procedures) Act of 1986. Eighteen male Sprague-Dawley rats aged 3 weeks were obtained from Charles River (Kent, UK) and housed immediately at thermoneutrality (c.28°C), on a high-fat diet (HFD; 45%, 824018 SDS, Kent, UK), under a 12:12-hour reverse light-dark cycle (lights off at 08:00, on at 20:00). These conditions were chosen so as to closer mimic human physiology [7], minimise animal stress and maximise data quality and translatability [10]. At 12 weeks of age, all animals were randomised to 4 weeks of standard housing temperature (20°C, n=6), YM-178 (28°C+β3, 0.75mg/kg/day, n=6) administration or HFD controls (28°C, n=6) from 12 weeks of age. In adherence to the NC3Rs, this experiment was ran alongside our work looking at the effect of exercise training on 'browning' and utilised the same cohort of control HFD animals.

Metabolic cages

All animals were placed in an open-circuit calorimeter (CLAMS: Columbus Instruments, Linton Instrumentation, UK) for 48h towards the end of the study. Assessment of whole body metabolism was carried out as previously described [11], after which all animals were weighed and fasted overnight prior to euthanasia by rising CO_2 gradient. BAT, perivascular BAT (PVAT) and IWAT were then rapidly dissected, weighed, snap-frozen in liquid nitrogen and stored at -80°C for subsequent analysis.

Gene expression analysis

Total RNA was extracted from each fat depot using the RNeasy Plus Micro extraction kit (Qiagen, West Sussex, UK) using an adapted version of the single step acidified phenol-chloroform method. RT-qPCR was carried out as previously described [11] using rat-specific oligonucleotide primers (Sigma) or FAM-MGB Taqman probes [11]. Gene expression was determined using the GeNorm algorithm against two selected reference genes;

RPL19:RPL13a in BAT and IWAT (stability value M = 0.163 in BAT and 0.383 in IWAT) and RPL19:HPRT1 in PVAT (stability value M = 0.285).

Serum analysis

Serum was thawed gently on ice with concentrations of glucose (GAGO-20, Sigma Aldrich, Gillingham, UK), triglycerides (LabAssay ™ Trigylceride, Wako, Neuss, Germany), non-esterified fatty acids (NEFA-HR(2), Wako, Neuss, Germany), insulin (80-INSRT-E01, Alpco, Salem, NH, USA) and leptin (EZRL-83K, Merck, Darmstadt, Germany) measured following manufacturer's instructions.

Mass spectrometry

Protein extraction, clean up and trypsinisation was carried out as previously described [11]. Briefly, 50-100 mg of frozen tissue was homogenised in 500 µL CellLytic MT cell lysis buffer (Sigma, C3228) prior to removal of lipid and other contaminants using the ReadyPrep 2D cleanup Kit (Biorad, 1632130). Samples were then subjected to reduction, alkylation and overnight trypsinisation following which they were dried down at 60°C for 4 h and stored at 80°C before resuspension in LCMS grade 5% acetonitrile in 0.1% formic acid for subsequent analysis. Analysis by mass spectrometry was carried out as previously described on a SCIEX TripleTOF 6600 instrument [12]. Briefly, samples were analysed in both SWATH (Data Independent Acquisition) and IDA (Information Dependent Acquisition) modes for quantitation and spectral library generation respectively. IDA data was searched together using ProteinPilot 5.0.2 to generate a spectral library and SWATH data was analysed using Sciex OneOmics software [13] extracted against the locally generated library as described previously [11].

2.6 Statistical analysis

Statistical analysis was performed in GraphPad Prism version 8.0 (GraphPad Software, San Diego, CA). Data are expressed as Mean±SEM with details of specific statistical tests in figure legends. Functional analysis of the proteome was performed using the Advaita

Bioinformatic iPathwayGuide software (www.advaitabio.com/ipathwayguide.html) (fold change ± 0.5 and confidence score cut-off of 0.75). Significantly impacted biological processes, molecular interactions and pathways were analysed in the context of pathways obtained from the Kyoto Encyclopaedia of Genes and Genomes (KEGG) database (Release 84.0+/10-26, Oct 17) [14] and the Gene Ontology Consortium database (2017-Nov) [15]. The Elim pruning method, which removes genes mapped to a significant GO term from more general (higher level) GO terms, was used to overcome the limitation of errors introduced by considering genes multiple times [16].

Results

Exposure to standard housing temperature drives weight gain and adiposity

Four weeks of exposure to 20°C increased weight gain and body weight with greater IWAT and BAT mass, an effect not seen with YM-178 (Fig. 1A-E). When body mass was incorporated into an ANCOVA, there was a significant relationship between body mass and energy expenditure (r^2 0.926, p=0.038, Fig.1F) and body mass and energy intake (r^2=0.852, p=0.025, Fig. 1H) in animals exposed to standard housing temperatures, whilst there was a change in the direction of the relationship between body mass and energy intake in animals treated with YM-178 (Fig. 1H). Cold-exposed animals exhibited an increase in light-phase, and a reduction in dark-phase ambulatory activity which was also seen in animals treated with YM-178 (Fig. 1G). There was no change in serum metabolites (i.e. glucose, triglycerides and NEFA) or hormones (i.e. insulin and leptin) (Fig. 1I-N).

Next, we analysed a panel of primary thermogenic genes in BAT and PVAT as we have previously shown these two anatomically and developmentally distinct BAT depots exhibit a divergent response to both a brief period of nutrient excess and exercise training [9, 11]. Despite an increase in BAT mass with cold, there was no reduction in thermogenic genes

(i.e. UCP1) in this depot or in PVAT with either cold or YM-178 (Fig. 2A-B). Expression of the BAT marker CITED1 and beige marker TMEM26 were reduced in BAT of both cold exposed and YM-178 treated animals whilst the beige marker P2RX5 was upregulated in PVAT of both groups. Using targeted arrays to screen for key genes involved in adipose tissue metabolism we saw an increase in the expression of FASN mRNA in both BAT and PVAT but not IWAT following cold exposure (Fig. 2A-C). There was also an increase of genes involved in glycolysis (i.e. HK2 and PDK), fatty acid oxidation (i.e. ACACA and ACACB) and insulin resistance (i.e. AdipoR1 and MAPK9) in PVAT only following cold exposure (Fig. 2D-K). This suggests that the metabolic response to cold in PVAT is uncoupled from BAT activation. We then analysed the same panel of thermogenic genes in IWAT to assess the 'browning' capacity of each intervention (Fig. 2C). UCP1 mRNA was absent in IWAT of all animals and, despite a c.125% increase in IWAT mass of cold exposed animals, there was no change in the expression of other key genes associated with thermogenesis (i.e. ADRβ3), beige adipocytes (i.e. TMEM26) or lipogenesis (i.e. FASN).

Identification of differentially regulated proteins in BAT and WAT associated with cold-induced increases in fat mass

Given the increase in BAT and IWAT mass seen in response to standard housing temperature, we carried out proteomic analysis to elucidate potential contributors to this physiological response identifying 175 differentially regulated proteins in BAT of cold-exposed animals (Table 1 for top 20 proteins, Supp. Data for full list). This method, which quantifies the 30-40% most abundant proteins across samples, did not detect UCP1 in BAT. There was, however, an increase in numerous other metabolic proteins in BAT of cold exposed animals including a pronounced increase in the mitochondrial citrate transporter proteins (SLC25a1), together with glucose-6-phosphate dehydrogenase (G6PD), phosphogluconate dehydrogenase (PGD), succinate dehydrogenase complex flavoprotein

subunit a (SDHA), fatty acid binding protein 5 (FABP5) and the muscle isoforms of phosphoglycerate mutase (PGAM2) and creatine kinase (CKm). The increase in these metabolic proteins occurred alongside a downregulation of proteins involved in the import of membrane (TIMM9) and cytoplasmic (TIMM13) proteins to the inner mitochondrial membrane, mitochondrial amino acid production (BCAT2) and redox state (PRDX4, GLRX3 and SOD2).

Conversely, 137 proteins were differentially regulated in BAT of YM-178 treated animals (Table 1 for top 20 significant proteins, Supp. Data for full list), with an upregulation in proteins involved in skeletal muscle physiology including myosin heavy chain 4 (MYH4) and light chain 12a (MYL12a), the fast-twitch skeletal muscle isoforms troponin I2 (TNNI2) and calsequestrin 1 (CASQ1) and myoglobin (MB) in addition to proteins governing endothelial adhesion and vascular growth (PECAM1 and FBLN5). These changes occurred alongside a downregulation of the aldo-keto reductase family member proteins B15 (AKR1B15) and C3 (AKR1C3) in addition to mevalonate diphosphate decarboxylase (MVD), trans-2,3-enoyl-CoA reductase (TECR), acyl-CoA dehydrogenase short/branched chain (ACADSB), phosphate cytidylyltransferase 1, choline, alpha (PCYT1A) and 3-hydroxybutyrate dehydrogenase 1 (BDH1) proteins indicating that YM-178 may be driving a muscle phenotype whilst perturbing steroid, cholesterol, acyl-CoA and phosphatidylcholine biosynthesis in BAT.

In IWAT, we detected 116 proteins differentially regulated in cold-exposed animals (Table 2 for top 20 significant proteins, Supp. Data for full list) with the upregulation of numerous lipid metabolic proteins including fatty acid binding proteins 1 (FABP1) and 3 (FABP3), fatty acid synthase (FASN) and ATP citrate lyase (ACLY) as well as those involved in beta oxidation including hydroxynacyl-CoA dehydrogenase (HADH), hydroxyacyl-CoA dehydrogenase trifunctional multienzyme complex subunit beta (HADHB) and acyl-CoA dehydrogenase long chain (ACADL). In addition, there was an upregulation of glycerol kinase (GK), pyruvate carboxylase (PC) and monocarboxylic acid transporter 1 (MCT1) and these alterations in

IWAT metabolism were accompanied by a downregulation of multiple proteins involved in mRNA processing and splicing (i.e. RNA binding motif protein 8B, RBM8B; dexd-Box helicase 39B, DDX39B and poly(u) binding splicing factor 60, PUF60).

YM-178 administration modulated 206 proteins in IWAT (Table 2 for top 20 significant proteins, Supp. Data for full list) including an upregulation of multiple proteins involved in the nervous system including synuclein Gamma (SNCG), neurolysin (NLN) and neuronal pas domain protein 4 (NPAS4). This was associated with an increase in proteins involved in lipid and cholesterol metabolism including carnitine palmitoyltransferase 1A (CPT1A), hormone-sensitive lipase (LIPE) and apolipoprotein C1 and M (APOC1 and APOM) in addition to solute carrier family 2 member 4 (GLUT4) and ATP synthase 5MG (ATP5MG). Interestingly, YM-178 also induced an increase in multiple inflammatory proteins in IWAT including orosomucoid 1 (ORM1), complement C4A (C4A), S100 calcium binding protein A8 (S100A8) and S100 calcium binding protein B (S100B). These metabolic and inflammatory alterations in IWAT were associated with a downregulation of multiple ribosomal proteins including ribosomal protein S21 (RPS21), ribosomal protein L32 (RPL32) and ribosomal protein L10a (RPL10a).

Functional analysis of the BAT and WAT proteome

We then carried out functional analysis of the BAT and IWAT proteome in order to elucidate potential biological processes, functions and pathways in adipose tissue that may be contributing to the significant increase in BAT and IWAT mass seen following cold-exposure.

The differentially regulated proteins in BAT of cold exposed animals enriched GO terms involved '*glucose import*', '*ATP-dependent helicase activity'* and '*regulation of protein phosphorylation'* whilst there was also an enrichment of nuclear related GO terms including '*histone deacetylation'*, '*nucleosomal DNA binding'*, '*nuclear chromatin'* and the '*nucleosome'* (Table 3, Fig. 3A-C). Conversely, differentially regulated proteins in BAT of animals treated

with YM-178 enriched GO terms including '*positive regulation of protein kinase B signalling'*, '*negative regulation of cellular carbohydrate metabolic process'* and '*positive regulation of atpase activity'* whilst there was also an enrichment of GO terms involved in both brown adipocyte and muscle biology including '*brown fat cell differentiation'*, '*skeletal muscle contraction'* and '*regulation of muscle contraction'* (Table 3, Fig. 3D-F). Finally, impact analysis demonstrated that the *'glycosaminoglycan degradation', 'notch signalling'* and *'glycosphingolipid biosynthesis – ganglio series'* pathways were affected by cold-exposure whilst YM-178 impacted pathways involved in *'Galactose metabolism'* and *'Hepatitis C'* (Table 4, Fig. 5A-F).

Differentially regulated proteins in IWAT of cold-exposed animals enriched GO terms involved in the '*DNA damage response', '3-hydroxyacyl-coa dehydrogenase activity'* and '*NAD+ binding'* whilst YM-178 enriched inflammatory terms including the *'acute phase response'* and *'structural constituent of ribosome'* suggesting an effect of sympathetic activation on both the inflammatory system and protein synthesis (Table 5, Fig. 4A-F). Impact analysis, meanwhile, demonstrated that cold-exposure was associated with an impact on both retinol and tyrosine metabolic pathways (Table 6, Fig. 6A-B). Conversely, YM-178 treatment impacted the *'ribosome'* pathway in addition to HIF-1 signalling and cytokine-cytokine receptor pathways (Table 6, Fig. 6C-D).

Elucidating the 'interactome' in BAT and IWAT

We then sought to discover putative hub proteins and signalling pathways in these tissues, through characterisation of the 'interactome' through protein-protein interactions. Differentially regulated proteins in BAT of cold-exposed animals were involved in 22 networks (i.e. the 'continent' and 21 'islands') with the 'continent' consisting of 293 interacting proteins. We identified multiple hub proteins in this network including the G proteins G protein subunit alpha I3 (GNAI3) and G protein subunit alpha Q (GNAQ), protein

tyrosine phosphatase non-receptor type 11 (PTPN11), actin gamma 1 (ACTG1) and serine/threonine kinase 24 (STK24) (Fig. 7A). Further analysis demonstrated that these hub proteins interacted with numerous other G proteins (i.e. Adenosine A1 receptor, ADORA1; Free fatty acid receptor 3, FFAR3 and neuropeptide Y receptor 2R; NPY2R), in addition to proteins involved in growth signalling pathways (i.e. phosphoinositide-3-kinase regulatory subunit 2; PIK3R2) and adipogenesis (platelet derived growth factor receptor beta; PDGFRB) to enrich 48 biological processes (Supp. Data) including 'anatomical structure involved in morphogenesis', 'developmental growth' and 'ER nucleus signalling pathway' and 26 molecular functions (Supp. Data) including exonuclease activity, steroid dehydrogenase activity, lipase activity and neuropeptide hormone activity. Conversely, differentially regulated proteins in BAT of YM-178 treated animals were involved in 17 networks, with the 'continent' consisting of 725 proteins. Hub proteins in this main network included multiple ribosomal proteins (i.e. ribosomal protein L5 (RPL5) and ribosomal protein L17 (RPL17)), proliferating cell nuclear antigen (PCNA), signal transducer and activator of transcription 3 (STAT3) and proteasome subunit alpha 4 (PSMA4) (Fig. 7B). These hub proteins were shown to interact with numerous other ribosomal (i.e. RPL10a and RPS23) and mitochondrial ribosomal proteins (i.e. MRPS9 and MRPL13) in addition to proteins involved in cytokine signalling (i.e. SOCS1, SOCS3 and STAT1/3 and 5B) and metabolism (i.e. LEP and MTOR) to enrich 30 processes including 'generation of neurons', 'cytokine biosynthetic process' and 'generation of precursor metabolites and energy' and 23 functions including 'RNA binding' and 'transcription cofactor activity' (Supp. Data).

Differentially regulated proteins in IWAT of cold-exposed animals created 12 networks with the continent consisting of 153 interacting proteins. Hub proteins in this main network included heterogeneous nuclear ribonucleoprotein k (HNRNPK), signal transducer and activator of transcription 5A (STAT5A), RNA binding motif protein 8A (RBM8A) and histone deacetylase 1 (HDAC1) (Fig. 8A). We show these hub proteins interact with other ribonucleotide and splicing factors (i.e. small nuclear ribonucleoprotein polypeptides B And

B1; SNRPB and serine and arginine rich splicing factor 1; SRSF1) in addition to proteins involved in adipogenesis (i.e. PDGFRB) and adipose tissue hypertrophy (i.e. LEP and LEPR) with the total network enriching 37 processes including 'RAS protein signal transduction' and 'activation of JUN kinase activity' and 21 functions including 'nucleotide binding' and 'DNA binding' (Supp. Data). Conversely, the main network in IWAT of YM-178 treated animals consisted of 819 interacting proteins with numerous ribosomal (i.e. RPL17, RPL18 and RPL6) and proteasomal (i.e. PSMA4, PSMA2 and PSMB10) proteins in addition to STAT5B and growth factor receptor bound protein 2 (GRB2) constituting the main hub proteins (Fig. 8B). Again, we showed these hub proteins in YM-178 treated animals interact with numerous other ribosomal (i.e. RPL10a and RPS29) and mitochondrial ribosomal proteins (i.e. MRPL1 and MRPL13), in addition to multiple tyrosine kinases (i.e. Fms related tyrosine kinase 1; FLT1 and Fms related tyrosine kinase 4; FLT4) with this network of interacting proteins enriching processes including 'Chromatin assembly or disassembly' and 'Cytokine biosynthetic process' and functions including 'RNA binding' and 'regulation of DNA dependent transcription and elongation' (Supp. Data).

Discussion

Housing temperature, especially cold exposure, impacts on metabolic homeostasis as illustrated by the effects it has on BAT and 'browning'. However, much less is known on the effects of 'browning' interventions in animals maintained at thermoneutrality [2, 17]. Our major finding is that chronic exposure to a mild-cold stimulus (i.e. standard housing temperature) drives weight gain and the deposition of large quantities of subcutaneous adipose tissue in obese animals rather than the activation of BAT and subsequent weight-loss as would be expected. This effect is not seen in animals treated with the highly selective β3-agonist YM-178, suggesting it is independent of sympathetic activation and a direct effect of ambient temperature, pointing towards a novel mechanism whereby animals increase

body weight and fat mass in the absence of prior cold-stress to potentially reduce heat loss and thus defend body temperature.

Whilst we do not detect any change in energy expenditure and energy intake in animals exposed to 20°C, it is important to note that metabolic cages are not truly representative of the entire study period and that, even with an adaptation period, it is an artificial environment where changes in energy intake are not always be detected [18]. Furthermore, at 600-700g these animals are likely to be near the size limit of the metabolic cages, such that home cage systems would be better-suited to collect physiological data in these large animals. These issues could also explain the relationship between body weight and both energy expenditure and energy intake, which suggests a reduction in both as body mass increases though the opposite is true in animals treated with the β3-agonist YM-178. Nevertheless, there is accumulating evidence that, in the absence of adaptive thermogenesis, other mechanisms compensate in order to maintain body temperature. For instance, in UCP1 k/o mice, a reduction in BAT thermogenesis leads to a compensatory increase in shivering thermogenesis in skeletal muscle [19]. Similarly, when shivering thermogenesis is impaired in sarcolipin k/o mice, there is a compensatory increase in BAT activity [19]. In obese animals lacking BAT, there seems to be an entirely different homeostatic response to cold-stress where following BAT lipectomy, obese, cold-exposed rats gain weight and exhibit nearly a one fold increase in adipose tissue mass [20]. There is also evidence to suggest that intermittent cold-exposure (from 20°C to 4°C) over a period of days increases weight gain and adiposity and that this is associated with transient, intermittent increases in energy intake [21]. Although other mechanisms such as intestinal growth and increased fatty acid absorption [22] may also play a role the impact of BAT, lipectomy on the response to cold-exposure mirrors our own findings and would suggest a compensatory mechanism for heat production in obesity when adaptive thermogenesis is insufficient. Importantly, an increase of c. 0.5g in BAT and of c. 10g in IWAT cannot account for the c. 41g higher weight gain seen in the cold-exposed animals. Given that liver mass was not higher in cold-exposed

animals, and that the increase in IWAT was highest, we speculate that this weight is not due to increased organ mass but due an increase in mass of dermal adipose tissue, given the putative role of this depot in regulating insulation and this should be investigated in future studies. A useful comparison here could be the Siberian hamster where obesity, and weight loss, can be manipulated by photoperiod. In this model, reductions in fat mass initially occur independently of reductions in energy intake and subcutaneous AT mass is preserved, likely due to its insulative properties highlighting how, at least in the short term, changes in weight and fat mass can be uncoupled from energy balance [23].

Another potentially important finding of this study is that the increase in weight gain and subcutaneous AT mass seen in cold-exposed animals was not associated with impaired metabolic parameters (i.e. fasting glucose and lipids) or any discernible adipose tissue dysfunction. Here, chronic exposure to a mild cold stimulus seemingly drives a phenotypically healthy expansion of subcutaneous AT, increasing it by 125% compared to controls. By using proteomics, we were able to elucidate processes in both BAT and IWAT associated with this expansion of AT mass. An increase in genes that modulate metabolism, including those involved in glycolysis, the TCA cycle and lipogenesis, suggests that there is an increase in metabolic flux of these depots which ultimately results in net lipogenesis. In BAT, this is associated with an enrichment of GO terms associated with DNA metabolism (i.e. histone deacetylation) with CTBP1, HDAC1 and SIRT2 all previously shown to be negative regulators of lipogenesis by either binding or deacetylating PPARY [24-26]. In IWAT, we show an enrichment of proteins involved in retinol metabolism, a well-known pathway which drives both adipogenesis and lipogenesis which is dependent on an intact NAD+ binding motif [27]. The enrichment of multiple proteins involved in NAD+ binding suggests this pathway is intact and upregulated and may contribute to this increase in IWAT mass.

We were also able to elucidate the impact of sympathetic activation in the absence of any change in housing temperature by administering YM-178. This highly selective β3-agonist

increases BAT activity, whole body EE and induces 'browning' in humans [28-31]. Administration of YM-178 to mice for 4-6 weeks at similar dosage to this study (i.e. 0.8mg/kg) reduces fat mass, increases UCP1 in IWAT and glucose uptake in BAT at standard housing temperature (SHT) whilst driving atherosclerosis, through BAT lipolysis in ApoE-/- and LdlR-/- mice [32]. Here, we show YM-178 treatment in obese animals raised at thermoneutraility has no impact on thermogenesis although it does modulate specific proteins involved in cell differentiation and skeletal muscle contraction. YM-178 also impacted on proteins involved in the acute phase response and inflammation in both BAT and IWAT with many increasing in the latter. Taken together, this suggests that YM-178, when given to obese rats, acts negatively on adipose tissue by driving inflammatory processes. Another potentially important finding is that chronic YM-178 induces the downregulation of ribosomal proteins. Adrenergic agonists have previously been shown to modify protein synthesis in skeletal muscle but the effect of YM-178 has yet to be examined with human studies focussing on overactive bladder and associated symptoms [33, 34]. The physiological relevance of a reduction in ribosomal proteins, and perturbed proteins synthesis in IWAT with YM-178 treatment and, whether this translates to human patients is as yet unclear.

Elucidating protein-protein interactions (PPI) is an important step in understanding both communication between proteins following an intervention and the identification of novel signalling pathways. We have previously shown that ribosomal proteins are important hub proteins in PPI networks following exercise training and, in the present study, show that these also respond to YM-178 [9]. Furthermore, these interact with multiple other mitochondrial ribosomal proteins and proteins governing energy metabolism such as mTOR and leptin. The role, and physiological significance, of these adaptations in putative ribosomal regulated signalling pathways remain to be determined but may assist in our understanding of the sympathetic control of adipose tissue. In BAT, the identification of GNAI3 and GNAC as hub proteins is of particular interest given the role of GPCRs and the

Gq signalling pathway, in particular, given its role in inhibiting BAT metabolism and 'browning' [35].

Conclusion

We propose that chronic suppression of BAT from weaning, through the use of thermoneutral housing, changes the physiological response to cold in the obese state. Instead, these animals deposit adipose tissue and gain weight, an effect not seen with YM-178, suggesting a direct effect of temperature, whereby an insulative mechanism is recruited when a thermogenic response is absent.

Availability of data and material: The datasets used and analysed during the current study are available from the corresponding author on reasonable request.

Authors' contributions: P.A., H.B. and M.E.S. conceived the study and attained the funding; P.A. and M.E.S. developed and designed the experiments; P.A, J.E.L, I.L, A.K.M and D. J. B. performed the experiments; P.A., A.K.M. and D.J.B. analysed the data; P.A. and M.E.S. wrote the paper which was revised critically by D.J.B., H.B., F.J.P.E, and J.E.L. for important intellectual content. All authors read and approved the final manuscript.

References

1. Chechi, K., W. van Marken Lichtenbelt, and D. Richard, *Brown and beige adipose tissues: phenotype and metabolic potential in mice and men.* J Appl Physiol (1985), 2018. **124**(2): p. 482-496.
2. Gordon, C.J., *The mouse thermoregulatory system: Its impact on translating biomedical data to humans.* Physiol Behav, 2017. **179**: p. 55-66.
3. !!! INVALID CITATION !!! {}.
4. Cui, X., et al., *Thermoneutrality decreases thermogenic program and promotes adiposity in high-fat diet-fed mice.* Physiol Rep, 2016. **4**(10).
5. Dittner, C., et al., *At thermoneutrality, acute thyroxine-induced thermogenesis and pyrexia are independent of UCP1.* Mol Metab, 2019. **25**: p. 20-34.
6. Raun, S.H., et al., *Housing temperature influences exercise training adaptations in mice.* bioRxiv, 2019: p. 651588.
7. Kalinovich, A.V., et al., *UCP1 in adipose tissues: two steps to full browning.* Biochimie, 2017. **134**: p. 127-137.
8. de Jong, J.M.A., et al., *Human brown adipose tissue is phenocopied by classical brown adipose tissue in physiologically humanized mice.* Nature Metabolism, 2019. **1**(8): p. 830-843.
9. Aldiss, P., et al., *Exercise does not induce browning of WAT at thermoneutrality and induces an oxidative, myogenic signature in BAT.* bioRxiv, 2019: p. 649061.
10. Hawkins, P. and H.D.R. Golledge, *The 9 to 5 Rodent - Time for Change? Scientific and animal welfare implications of circadian and light effects on laboratory mice and rats.* J Neurosci Methods, 2018. **300**: p. 20-25.
11. Aldiss, P., et al., *Interscapular and Perivascular Brown Adipose Tissue Respond Differently to a Short-Term High-Fat Diet.* 2019.
12. Mele, L., et al., *A new inhibitor of glucose-6-phosphate dehydrogenase blocks pentose phosphate pathway and suppresses malignant proliferation and metastasis in vivo.* Cell Death Dis, 2018. **9**(5): p. 572.
13. Lambert, J.P., et al., *Mapping differential interactomes by affinity purification coupled with data-independent mass spectrometry acquisition.* Nat Methods, 2013. **10**(12): p. 1239-45.
14. Kanehisa, M., *The KEGG database.* Novartis Found Symp, 2002. **247**: p. 91-101; discussion 101-3, 119-28, 244-52.
15. Ashburner, M., et al., *Gene ontology: tool for the unification of biology. The Gene Ontology Consortium.* Nat Genet, 2000. **25**(1): p. 25-9.
16. Alexa, A., J. Rahnenfuhrer, and T. Lengauer, *Improved scoring of functional groups from gene expression data by decorrelating GO graph structure.* Bioinformatics, 2006. **22**(13): p. 1600-7.
17. Hylander, B.L. and E.A. Repasky, *Thermoneutrality, Mice, and Cancer: A Heated Opinion.* Trends Cancer, 2016. **2**(4): p. 166-175.
18. Lewis, J.E., et al., *Hypothalamic over-expression of VGF in the Siberian hamster increases energy expenditure and reduces body weight gain.* PLoS One, 2017. **12**(2): p. e0172724.
19. Rowland, L.A., et al., *Sarcolipin and uncoupling protein 1 play distinct roles in diet-induced thermogenesis and do not compensate for one another.* Obesity (Silver Spring), 2016. **24**(7): p. 1430-3.
20. Stern, J.S., et al., *Scapular brown fat removal enhances development of adiposity in cold-exposed obese Zucker rats.* Am J Physiol, 1984. **247**(5 Pt 2): p. R918-26.
21. Yoo, H.S., et al., *Intermittent cold exposure enhances fat accumulation in mice.* PLoS One, 2014. **9**(5): p. e96432.
22. Nilaweera, K.N. and J.R. Speakman, *Regulation of intestinal growth in response to variations in energy supply and demand.* Obes Rev, 2018. **19 Suppl 1**: p. 61-72.

23. Bartness, T.J. and C.K. Song, *Brain-adipose tissue neural crosstalk.* Physiol Behav, 2007. **91**(4): p. 343-51.
24. Kuzmochka, C., et al., *Inactivation of histone deacetylase 1 (HDAC1) but not HDAC2 is required for the glucocorticoid-dependent CCAAT/enhancer-binding protein alpha (C/EBPalpha) expression and preadipocyte differentiation.* Endocrinology, 2014. **155**(12): p. 4762-73.
25. Wang, F. and Q. Tong, *SIRT2 suppresses adipocyte differentiation by deacetylating FOXO1 and enhancing FOXO1's repressive interaction with PPARgamma.* Mol Biol Cell, 2009. **20**(3): p. 801-8.
26. Vernochet, C., et al., *C/EBPalpha and the corepressors CtBP1 and CtBP2 regulate repression of select visceral white adipose genes during induction of the brown phenotype in white adipocytes by peroxisome proliferator-activated receptor gamma agonists.* Mol Cell Biol, 2009. **29**(17): p. 4714-28.
27. Schupp, M., et al., *Retinol saturase promotes adipogenesis and is downregulated in obesity.* Proc Natl Acad Sci U S A, 2009. **106**(4): p. 1105-10.
28. Loh, R.K.C., et al., *Acute metabolic and cardiovascular effects of mirabegron in healthy individuals.* Diabetes Obes Metab, 2019. **21**(2): p. 276-284.
29. Baskin, A.S., et al., *Regulation of Human Adipose Tissue Activation, Gallbladder Size, and Bile Acid Metabolism by a beta3-Adrenergic Receptor Agonist.* Diabetes, 2018. **67**(10): p. 2113-2125.
30. Cypess, A.M., et al., *Activation of human brown adipose tissue by a beta3-adrenergic receptor agonist.* Cell Metab, 2015. **21**(1): p. 33-8.
31. Finlin, B.S., et al., *Human adipose beiging in response to cold and mirabegron.* JCI Insight, 2018. **3**(15).
32. Sui, W., et al., *Bladder drug mirabegron exacerbates atherosclerosis through activation of brown fat-mediated lipolysis.* Proc Natl Acad Sci U S A, 2019. **116**(22): p. 10937-10942.
33. Puzzo, D., et al., *CL316,243, a beta3-adrenergic receptor agonist, induces muscle hypertrophy and increased strength.* Sci Rep, 2016. **5**: p. 37504.
34. Emery, P.W., et al., *Chronic effects of beta 2-adrenergic agonists on body composition and protein synthesis in the rat.* Biosci Rep, 1984. **4**(1): p. 83-91.
35. Klepac, K., et al., *The Gq signalling pathway inhibits brown and beige adipose tissue.* Nat Commun, 2016. **7**: p. 10895.

Figure legends

Figure 1. Cold exposure (20°C) but not YM-178 (28°C+β3) drove weight gain and deposition of BAT and inguinal white adipose tissue (IWAT) with no effect on serum metabolites. (A) Final body weight, (B) 4 week intervention weight gain, (C) total fat mass, (D) BAT mass, (E) IWAT mass, (F) 24h oxygen consumption, (G) 24h ambulatory activity, (H) 24h energy intake, (I-N) serum hormones and metabolites. Data expressed as mean ± SEM, n=4-5 per group. For comparison, data was analysed by either one (A-E and H-O) or two-way ANOVA (F-G) with Sidak post-hoc tests. Significance denoted as * <0.05; ** <0.01 or *** <0.001.

Figure 2. Cold exposure (20°C) and YM-178 (28°C+β3) do not impact key thermogenic genes. (A-C) Markers of brown and beige adipose tissue in BAT, PVAT and IWAT, (D-K) select metabolic genes in BAT and PVAT. For comparison, data was analysed one-way ANOVA with Sidak post-hoc tests.

Figure 3. Overview of enriched gene ontology (GO) terms in BAT following cold-exposure ((20°C), B and C) and YM-178 treatment (28°C+β3, D-F). (A) Venn diagram of differentially regulated protein, (B) Histone deacetylation, (C) Enhancer sequence-specific DNA binding, (D) Skeletal muscle contraction, (E) Brown fat cell differentiation, (F) Glucocorticoid receptor binding and (G-F) terms enriched in both groups, (G) Protein tyrosine kinase activity and (H) Positive regulation of autophagy in mitochondrion. Figures created with AdvaitaBio IPathwayGuide.

Figure 4. Overview of enriched gene ontology (GO) terms in IWAT following cold-exposure (20°C, B and C) and YM-178 treatment (28°C+β3, D-F). (A) Venn diagram of differentially regulated protein, (B) DNA damage response, (C) 3-hydroxyacyl-CoA dehydrogenase activity, (D) NAD+ binding, (E) Acute phase response and (F) Structural constituent of ribosome. Figures created with AdvaitaBio IPathwayGuide.

Figure 5. Overview of significantly impacted pathways in BAT following cold-exposure (20°C, A-C) and YM-178 treatment (28°C+β3, D-F). (A) Glycosaminoglycan degradation, (B) Notch pathway, (C) Glycoshingolipid biosynthesis ganglio series, (D) Galactose metabolism, (E) Hepatitis C and (F) Amino and sugar nucleotide sugar metabolism. Figures created with AdvaitaBio IPathwayGuide.

Figure 6. Overview of significantly impacted pathways in IWAT following cold-exposure (20°C, A-C), YM-178 treatment (28°C+β3, C) and in both groups (E). (A) Retinol metabolism, (B) Tyrosine metabolism, (C) Hif1a signaling, (D) Ribosome, (E) Spliceosome. Figures created with AdvaitaBio IPathwayGuide.

Figure 7. Protein-protein interaction network or differentially regulated proteins in BAT following cold-exposure (20°C, A) and YM-178 treatment (28°C+β3, B) with hub proteins in bold. Figures created with NetworkAnalyst.

Figure 8. Protein-protein interaction network or differentially regulated proteins in IWAT following cold-exposure (20°C, A) and YM-178 treatment (28°C+β3, B) with hub proteins in bold. Figures created with NetworkAnalyst.

Tables

Table 1: Differentially regulated proteins in BAT

GeneID	Protein name	logfc	adjpv
20°C			
80754	Rabep2	3.69	6.35E-05
114122	Vcan	2.74	0.000269
292073	Galns	-2.75	0.00027
64012	Rad50	1.50	0.000288
171139	Timm9	-1.94	0.00037
295088	Gmps	0.67	0.000396
81716	Ggcx	1.44	0.000639
25622	Ptpn11	-2.47	0.000975
289590	Ociad1	-1.41	0.000988
29384	H2afy	-1.15	0.001077
302669	Ca5b	1.18	0.001237
499991	Steap4	-3.88	0.00228
315265	Twf1	-1.54	0.00248
25283	Gclc	2.57	0.002571
84474	Ddx1	2.23	0.00326
94342	Bag6	-1.26	0.0036
89827	Ddx39a	1.26	0.00397
64679	Tgm4	0.95	0.00616
64517	Thop1	1.25	0.006186
29743	Slc25a1	1.10	0.006388
28°C+ β3			
116689	Ptpn6	-3.56	0.000154
25650	Atp1b1	-1.40	0.000303
59108	Mb	2.71	0.000548
306262	Btd	2.72	0.000735
501167	Gmppa	1.58	0.000934
64528	Golga2	0.98	0.001723
287633	Lrrc59	-0.62	0.002902
81726	Mvd	-3.82	0.004012
363425	Cav2	-2.41	0.004547
114559	Arhgef7	-1.54	0.005187
25737	Pcna	1.41	0.005462
171516	Akr1c3	-3.61	0.006199
311328	Rmdn3	-2.54	0.006373
312398	Smarcad1	-2.97	0.006491
29583	Pecam1	3.43	0.006613
25491	Nes	-1.35	0.008957
25106	Rgn	1.79	0.009092
117099	Bdh1	-1.76	0.009659

1E+08	LOC100364457	0.98	0.010813
681429	Rps27l	1.68	0.011212

Table 2: Differentially regulated proteins in WAT

GeneID	Protein name	logfc	adjpv
20°C			
117028	Bin1	-2.79	8.97E-06
304290	Kdelr2	-2.68	4.47E-05
24667	Ppm1b	-2.65	0.000108
84114	Agps	-1.35	0.000125
84401	Puf60	-2.94	0.000753
300983	Abhd14b	0.94	0.000791
29218	Rcn2	-2.40	0.000854
290028	Osgep	-0.94	0.002064
24230	Tspo	-2.34	0.00248
171452	Rab3il1	-2.15	0.00629
84355	Atox1	-0.89	0.007345
311428	RGD1311739	1.07	0.007461
25246	Bsg	0.84	0.007876
25027	Slc16a1	1.02	0.008061
361999	Anp32e	-3.03	0.00862
24788	Sord	0.81	0.01132
301384	Hibch	1.64	0.013339
83576	Sort1	0.96	0.014054
29666	Psmb6	0.72	0.017559
28°C+ β3			
83730	Vamp8	-3.75	6.93E-05
29521	Scamp1	1.51	0.000111
25116	Hsd11b1	0.92	0.000382
117045	Eif4e	-0.69	0.000942
25342	Oxtr	1.79	0.001104
298566	C1qa	0.85	0.001124
445268	Ufc1	-0.65	0.001133
78947	Gcs1	0.61	0.00204
266734	Npas4	0.87	0.004234
246303	Serbp1	0.78	0.004516
25139	Slc2a4	1.36	0.005653
619574	LOC619574	-1.74	0.006446
64317	Gpx3	1.00	0.006558
84474	Ddx1	-0.73	0.007131
24471	Hspb1	1.26	0.007327

170673	Palm	2.47	0.007749
313035	Dnajc8	-2.09	0.008094
64045	Glrx	-3.30	0.008229
122799	Rps25	-1.04	0.009005
252928	Timm13	-0.62	0.009087

Table 3. GO terms enriched in BAT

goId	goName	countDE	countAll	pv_elim
20°C				
Biological Process				
GO:0016575	histone deacetylation	4	5	0.0047
GO:0000122	negative regulation of transcription from RNA polymerase II promoter	14	40	0.008
GO:0003006	developmental process involved in reproduction	20	68	0.0146
GO:0071786	endoplasmic reticulum tubular network organization	3	4	0.0209
GO:0019098	reproductive behavior	3	4	0.0209
GO:0006544	glycine metabolic process	3	4	0.0209
GO:0016226	iron-sulfur cluster assembly	3	4	0.0209
GO:0090068	positive regulation of cell cycle process	7	17	0.0231
GO:0046323	glucose import	6	14	0.0285
GO:0001932	regulation of protein phosphorylation	32	129	0.0316
Molecular Function				
GO:0000980	RNA polymerase II distal enhancer sequence-specific DNA binding	4	5	0.0046
GO:0030984	kininogen binding	3	3	0.006
GO:0031492	nucleosomal DNA binding	4	6	0.0119
GO:0001846	opsonin binding	3	4	0.0207
GO:0005212	structural constituent of eye lens	3	4	0.0207
GO:0016634	oxidoreductase activity, acting on the CH-CH group of donors, oxygen as acceptor	3	4	0.0207
GO:0016831	carboxy-lyase activity	5	10	0.022
GO:0016746	transferase activity, transferring acyl groups	9	25	0.0259
GO:0004616	phosphogluconate dehydrogenase (decarboxylating) activity	2	2	0.0331
GO:0008484	sulfuric ester hydrolase activity	2	2	0.0331
Cellular Component				
GO:0042582	azurophil granule	4	4	0.0011
GO:0000790	nuclear chromatin	12	27	0.0014
GO:0031616	spindle pole centrosome	3	4	0.0209
GO:0000786	nucleosome	5	10	0.0223
GO:0042719	mitochondrial intermembrane space protein transporter complex	2	2	0.0333
GO:0001740	Barr body	2	2	0.0333
GO:0072687	meiotic spindle	2	2	0.0333
GO:0034751	aryl hydrocarbon receptor complex	2	2	0.0333

GO:0043196	varicosity	2	2	0.0333
GO:0001931	uropod	3	5	0.0453
28°C+ β3				
Biological Process				
GO:0003009	skeletal muscle contraction	5	7	0.0015
GO:0051897	positive regulation of protein kinase B signaling	6	11	0.0034
GO:0010677	negative regulation of cellular carbohydrate metabolic process	3	3	0.0039
GO:1901896	positive regulation of calcium-transporting ATPase activity	3	3	0.0039
GO:0032781	positive regulation of ATPase activity	9	15	0.0055
GO:0050873	brown fat cell differentiation	3	4	0.0138
GO:0006937	regulation of muscle contraction	8	22	0.0147
GO:0071560	cellular response to transforming growth factor beta stimulus	8	22	0.0147
GO:0060048	cardiac muscle contraction	6	15	0.0209
GO:0048193	Golgi vesicle transport	12	42	0.024
Molecular Function				
GO:0035259	glucocorticoid receptor binding	3	4	0.013
GO:0001671	ATPase activator activity	3	4	0.013
GO:0008134	transcription factor binding	15	55	0.016
GO:0050431	transforming growth factor beta binding	2	2	0.024
GO:0031730	CCR5 chemokine receptor binding	2	2	0.024
GO:0031014	troponin T binding	2	2	0.024
GO:0005044	scavenger receptor activity	3	5	0.029
GO:0019905	syntaxin binding	4	9	0.037
GO:0016779	nucleotidyltransferase activity	4	9	0.037
GO:0004888	transmembrane signaling receptor activity	4	9	0.037
Cellular Component				
GO:0005887	integral component of plasma membrane	12	32	0.002
GO:0030134	COPII-coated ER to Golgi transport vesicle	5	9	0.0067
GO:0005861	troponin complex	2	2	0.0245
GO:0001741	XY body	2	2	0.0245
GO:0043596	nuclear replication fork	3	5	0.0299
GO:0044295	axonal growth cone	3	5	0.0299
GO:0016459	myosin complex	5	13	0.0399

Table 4. Impacted pathways in BAT with SHT and YM-178

Pathway name	pv
20°C	
Glycosaminoglycan degradation	0.004999
Notch signaling pathway	0.031163
Glycosphingolipid biosynthesis - ganglio series	0.034463
28°C+ β3	
Galactose metabolism	0.024394
Hepatitis C	0.037178

Table 5. GO terms enriched in WAT

goId	goName	countDE	countAll	pv_elim
20°C				
Biological Process				
GO:0030330	DNA damage response, signal transduction by p53 class mediator	5	6	0.0022
GO:0048711	positive regulation of astrocyte differentiation	3	3	0.0023
GO:0071498	cellular response to fluid shear stress	3	3	0.0023
GO:0032780	negative regulation of ATPase activity	3	3	0.0023
GO:0051607	defense response to virus	5	9	0.003
GO:0001822	kidney development	11	35	0.0036
GO:0050731	positive regulation of peptidyl-tyrosine phosphorylation	7	17	0.0037
Molecular Function				
GO:0051287	NAD binding	11	31	0.0013
GO:0008144	drug binding	9	29	0.0101
GO:0005001	transmembrane receptor protein tyrosine phosphatase activity	2	2	0.0178
GO:0005521	lamin binding	3	5	0.0191
GO:0042393	histone binding	5	13	0.021
GO:0033613	activating transcription factor binding	3	6	0.0345
GO:0003857	3-hydroxyacyl-CoA dehydrogenase activity	3	6	0.0345
GO:0045296	cadherin binding	22	113	0.0365
GO:0004028	3-chloroallyl aldehyde dehydrogenase activity	2	3	0.0486
GO:0071933	Arp2/3 complex binding	2	3	0.0486
Cellular Component				
GO:0005884	actin filament	9	24	0.0021
GO:0032993	protein-DNA complex	5	11	0.0088
GO:0002102	podosome	7	14	0.013
GO:0016607	nuclear speck	8	26	0.0146
GO:0031209	SCAR complex	2	2	0.0172

GO:0042611	MHC protein complex	2	2	0.0172
GO:0005687	U4 snRNP	2	2	0.0172
GO:0005856	cytoskeleton	49	238	0.0284
GO:0030054	cell junction	41	216	0.0291
GO:0005681	spliceosomal complex	9	22	0.0311
28°C+ β3				
Biological Process				
GO:0006953	acute-phase response	7	12	0.0035
GO:0000381	regulation of alternative mRNA splicing, via spliceosome	7	12	0.0035
GO:0034113	heterotypic cell-cell adhesion	8	12	0.0061
GO:0070528	protein kinase C signaling	4	5	0.0063
GO:0015671	oxygen transport	4	5	0.0063
	positive regulation of myoblast fusion	3	3	0.0077
	CRD-mediated mRNA stabilization	3	3	0.0077
GO:0007566	embryo implantation	6	12	0.0179
GO:0040007	growth	29	103	0.0209
GO:0071345	cellular response to cytokine stimulus	25	86	0.0211
Molecular Function				
GO:0003735	structural constituent of ribosome	24	62	0.00037
GO:0005344	oxygen carrier activity	4	5	0.00657
GO:0003730	mRNA 3'-UTR binding	8	18	0.01548
GO:0003682	chromatin binding	10	25	0.01623
GO:0140097	catalytic activity, acting on DNA	5	9	0.01908
GO:0042162	telomeric DNA binding	3	4	0.02688
GO:0045294	alpha-catenin binding	3	4	0.02688
	exonuclease activity	3	4	0.02688
GO:0003723	RNA binding	73	281	0.02734
GO:0019825	oxygen binding	4	7	0.03278
Cellular Component				
GO:0022625	cytosolic large ribosomal subunit	15	30	0.00018
GO:0016323	basolateral plasma membrane	14	32	0.00164
	hemoglobin complex	3	3	0.00782
GO:0005903	brush border	10	23	0.00812
GO:0030864	cortical actin cytoskeleton	9	20	0.00918
GO:0016327	apicolateral plasma membrane	3	4	0.02666
GO:0044451	nucleoplasm part	18	58	0.0269
GO:0005637	nuclear inner membrane	5	10	0.03167
GO:0035770	ribonucleoprotein granule	11	32	0.03804
GO:0097225	sperm midpiece	2	2	0.03953

Table 6. Impacted pathways in WAT

Pathway name	**pv**
20°C	
Retinol metabolism	0.02255
Tyrosine metabolism	0.047604
28°C+ β3	
Ribosome	0.00024
HIF-1 signaling pathway	0.030833
Cytokine-cytokine receptor interaction	0.032493
Pancreatic cancer	0.03371
Hippo signaling pathway - multiple species	0.036124
Melanoma	0.041587

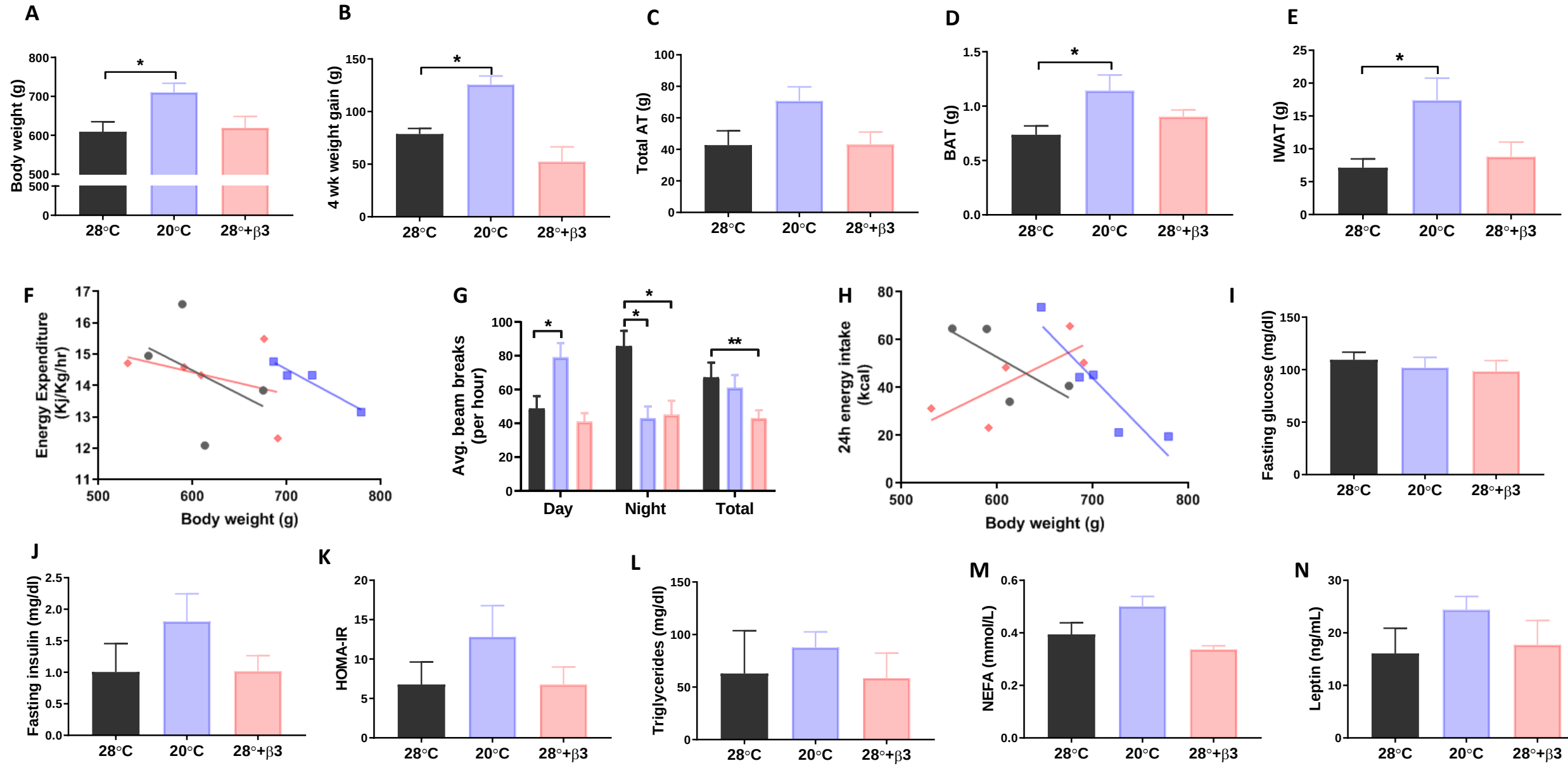
A
Body weight (g)
800
700
600
500
500
0
*
28°C
20°C
28°+β3
B
4 wk weight gain (g)
150
100
50
0
*
28°C
20°C
28°+β3
C
Total AT (g)
100
80
60
40
20
0
28°C
20°C
28°+β3
D
BAT (g)
1.5
1.0
0.5
0.0
*
28°C
20°C
28°+β3
E
IWAT (g)
25
20
15
10
5
0
*
28°C
20°C
28°+β3
F
Energy Expenditure (Kj/Kg/hr)
17
16
15
14
13
12
11
500
600
700
800
Body weight (g)
G
Avg. beam breaks (per hour)
100
80
60
40
20
0
*
*
*
**
Day
Night
Total
H
24h energy intake (kcal)
80
60
40
20
0
500
600
700
800
Body weight (g)
I
Fasting glucose (mg/dl)
150
100
50
0
28°C
20°C
28°+β3
J
Fasting insulin (mg/dl)
2.5
2.0
1.5
1.0
0.5
0.0
28°C
20°C
28°+β3
K
HOMA-IR
20
15
10
5
0
28°C
20°C
28°+β3
L
Triglycerides (mg/dl)
150
100
50
0
28°C
20°C
28°+β3
M
NEFA (mmol/L)
0.6
0.4
0.2
0.0
28°C
20°C
28°+β3
N
Leptin (ng/mL)
30
20
10
0
28°C
20°C
28°+β3

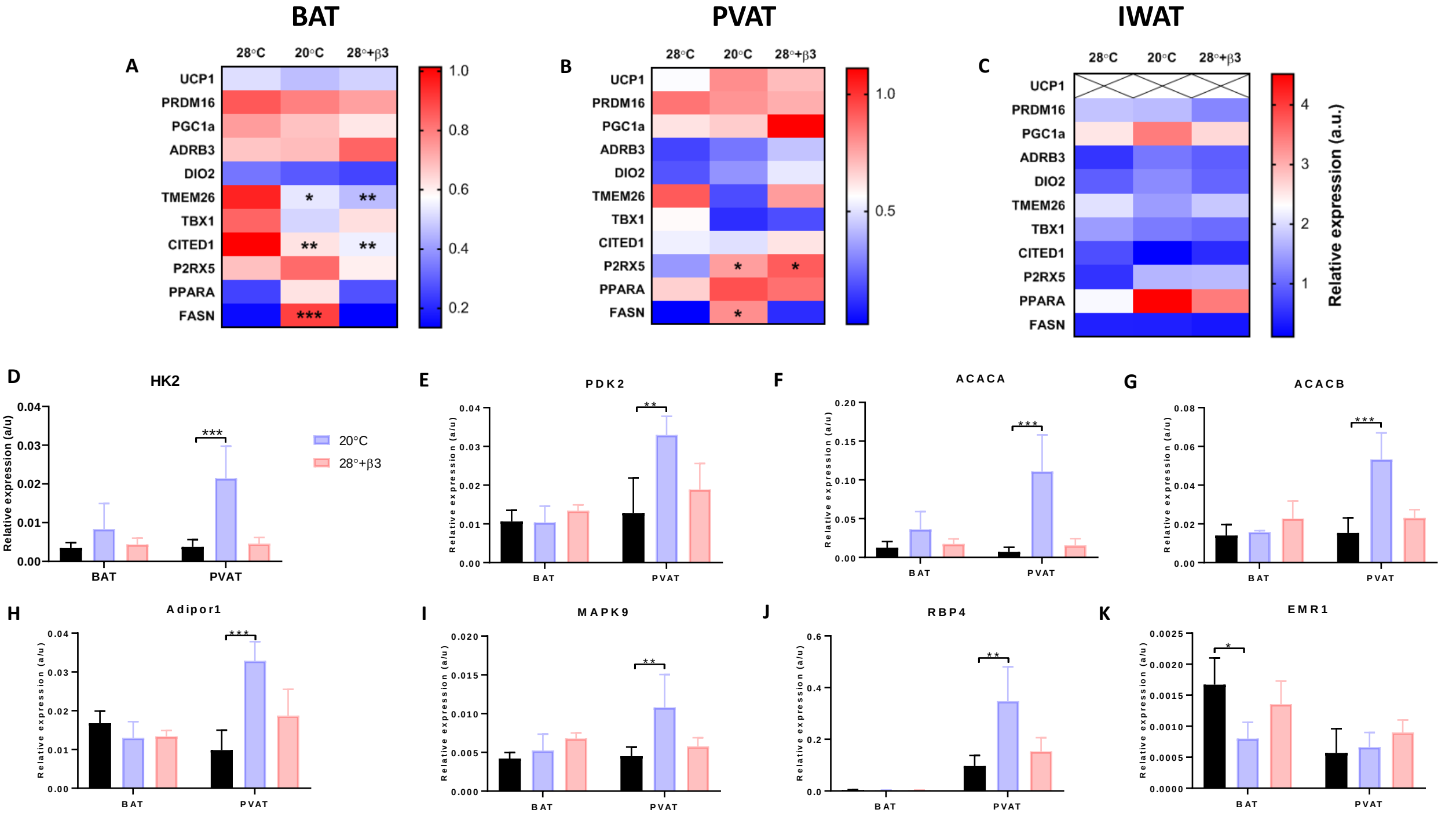
BAT
PVAT
IWAT
A
B
C
28°C
20°C
28°+β3
UCP1
PRDM16
PGC1a
ADRB3
DIO2
TMEM26
TBX1
CITED1
P2RX5
PPARA
FASN
Relative expression (a.u.)
D
HK2
E
PDK2
F
ACACA
G
ACACB
H
Adipor1
I
MAPK9
J
RBP4
K
EMR1
Relative expression (a/u)
20°C
28°+β3
BAT
PVAT

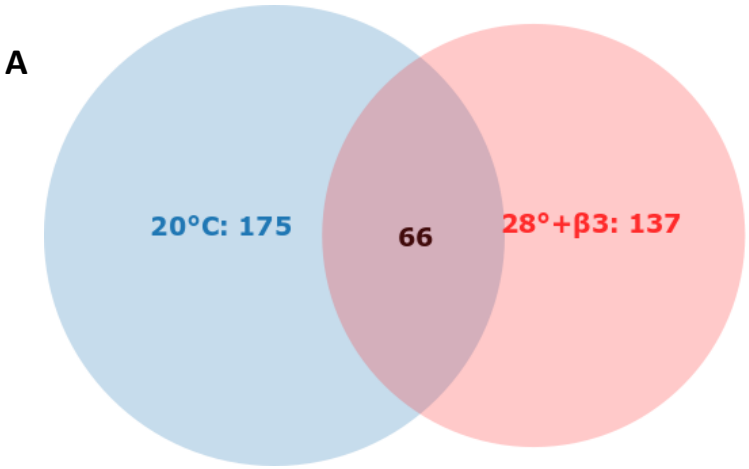
A
20°C: 175
66
28°+β3: 137

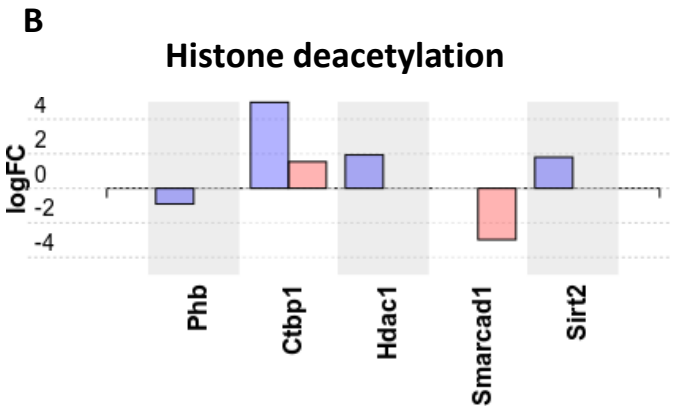
B
Histone deacetylation
logFC
4
2
0
-2
-4
Phb
Ctbp1
Hdac1
Smarcad1
Sirt2

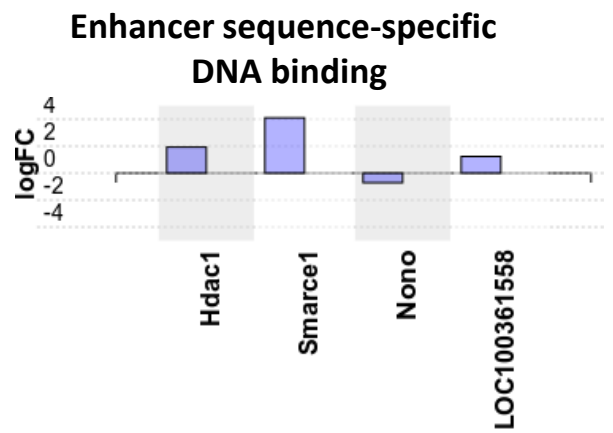
C
Enhancer sequence-specific DNA binding
logFC
4
2
0
-2
-4
Hdac1
Smarce1
Nono
LOC100361558

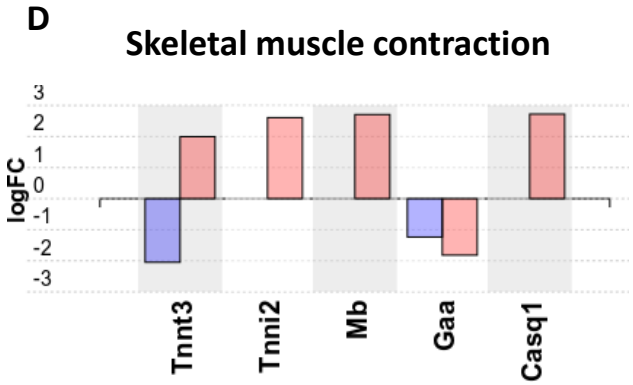
D
Skeletal muscle contraction
logFC
3
2
1
0
-1
-2
-3
Tnnt3
Tnni2
Mb
Gaa
Casq1

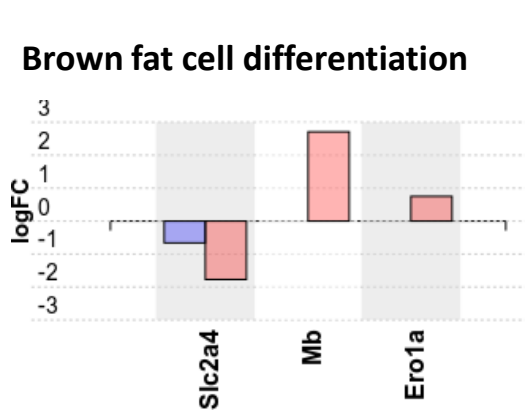
E
Brown fat cell differentiation
logFC
3
2
1
0
-1
-2
-3
Slc2a4
Mb
Ero1a

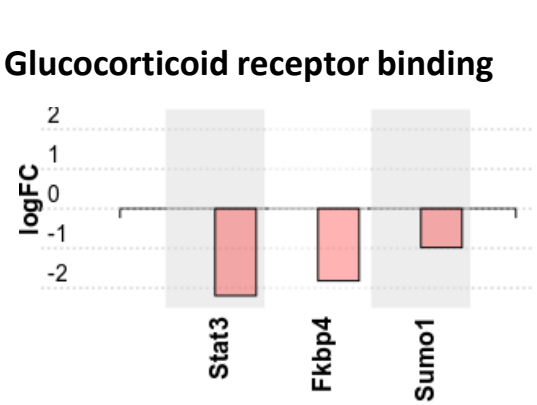
F
Glucocorticoid receptor binding
logFC
2
1
0
-1
-2
Stat3
Fkbp4
Sumo1

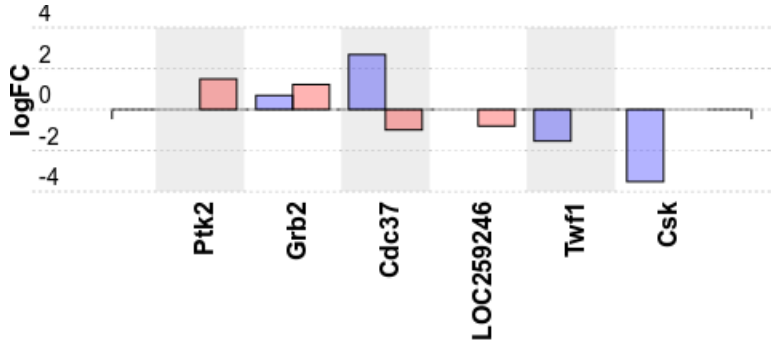
G
Protein tyrosine kinase activity
logFC
4
2
0
-2
-4
Ptk2
Grb2
Cdc37
LOC259246
Twf1
Csk


H
Pos. regulation of autophagy in mitochondrion
logFC
3
2
1
0
-1
-2
-3
Hk2
Cdc37

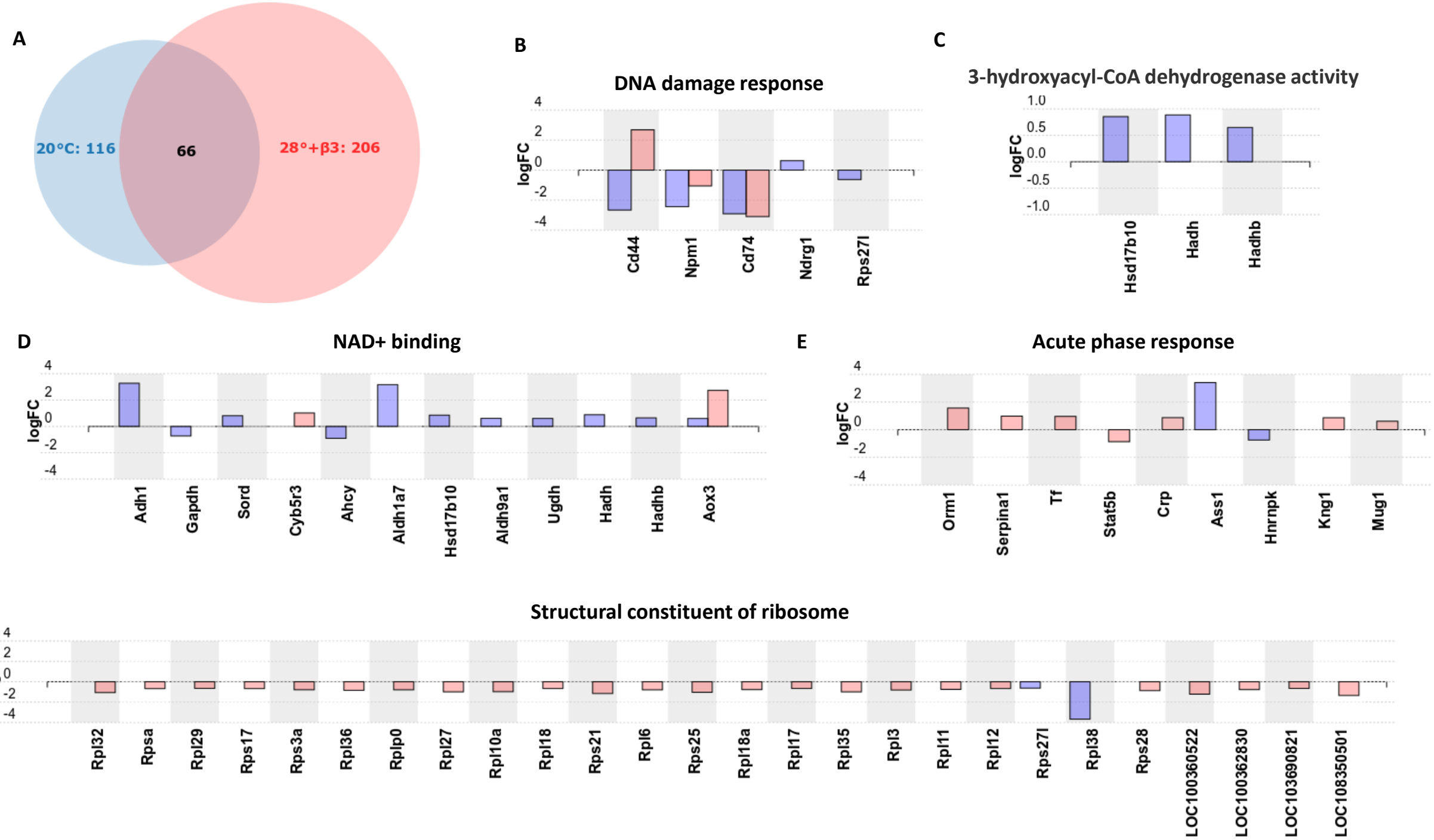
A
20°C: 116
66
28°+β3: 206
B
DNA damage response
logFC
4
2
0
-2
-4
Cd44
Npm1
Cd74
Ndrg1
Rps27l
C
3-hydroxyacyl-CoA dehydrogenase activity
logFC
1.0
0.5
0.0
-0.5
-1.0
Hsd17b10
Hadh
Hadhb
D
NAD+ binding
logFC
4
2
0
-2
-4
Adh1
Gapdh
Sord
Cyb5r3
Ahcy
Aldh1a7
Hsd17b10
Aldh9a1
Ugdh
Hadh
Hadhb
Aox3
E
Acute phase response
logFC
4
2
0
-2
-4
Orm1
Serpina1
Tf
Stat5b
Crp
Ass1
Hnrnpk
Kng1
Mug1
F
Structural constituent of ribosome
logFC
4
2
0
-2
-4
Rpl32
Rpsa
Rpl29
Rps17
Rps3a
Rpl36
Rplp0
Rpl27
Rpl10a
Rpl18
Rps21
Rpl6
Rps25
Rpl18a
Rpl17
Rpl35
Rpl3
Rpl11
Rpl12
Rps27l
Rpl38
Rps28
LOC100360522
LOC100362830
LOC103690821
LOC108350501

A Glycosaminoglycan degradation

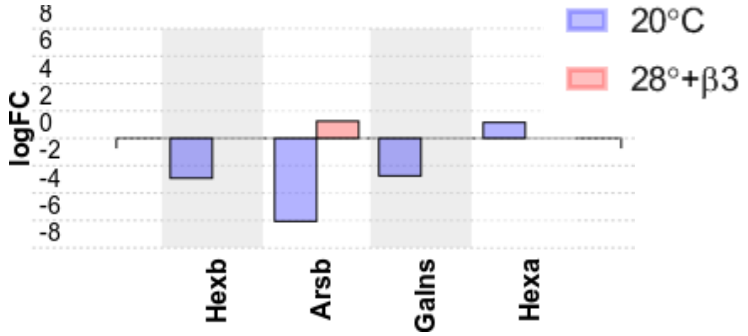

B Notch pathway

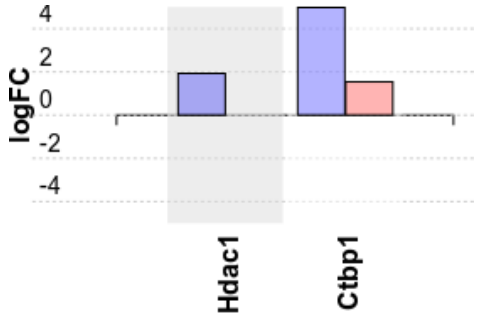

C Glycosphingolipid biosynthesis ganglio series

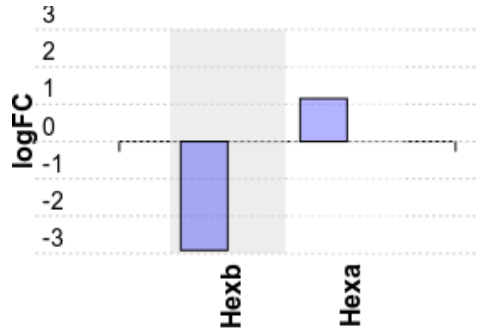

D Galactose metabolism

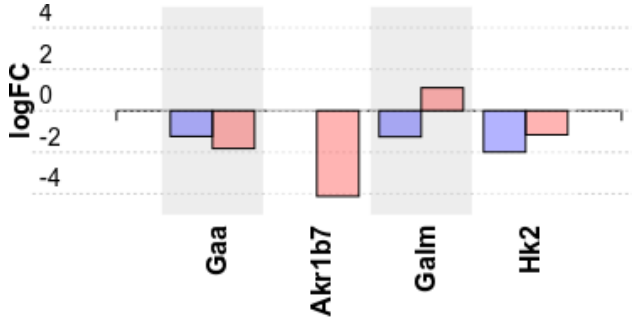

E Amino sugar and nucleotide sugar metabolism

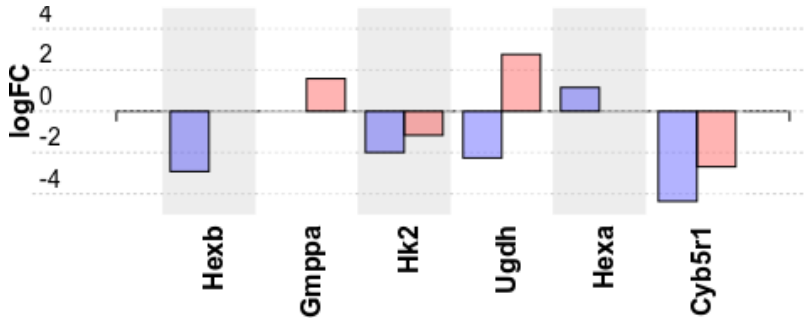

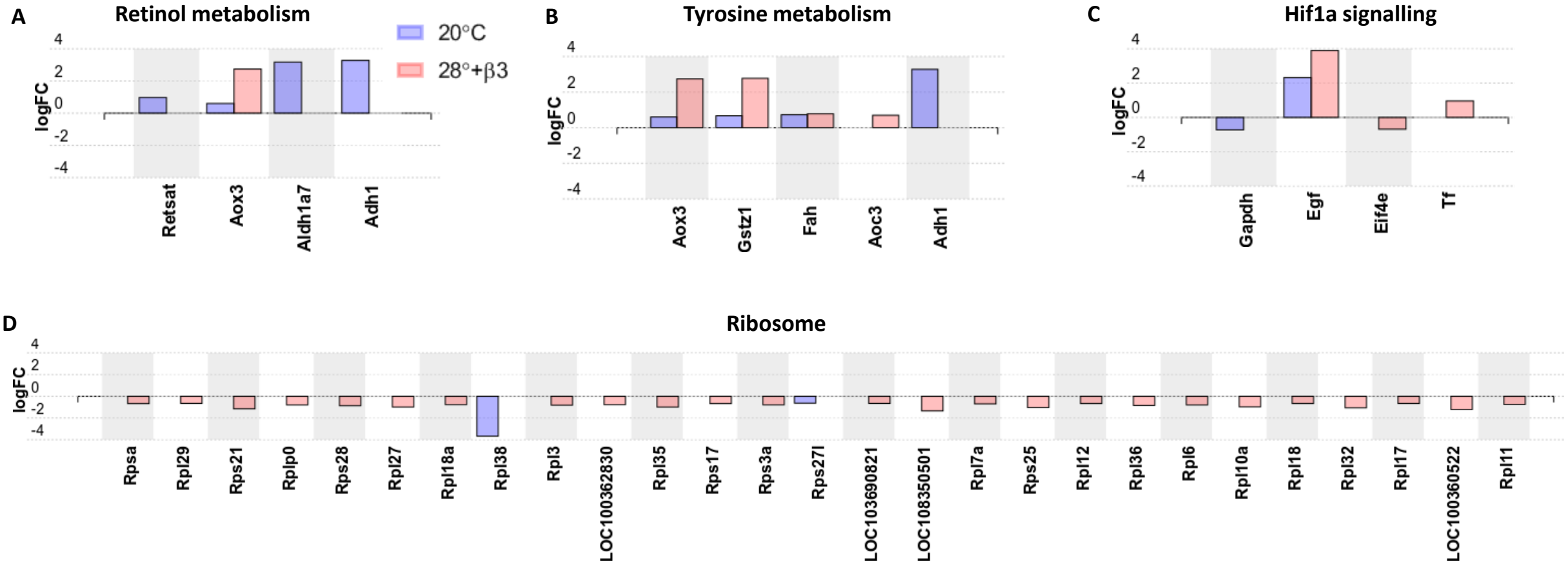
A
Retinol metabolism
20°C
28°+β3
logFC
4
2
0
-2
-4
Retsat
Aox3
Aldh1a7
Adh1
B
Tyrosine metabolism
logFC
4
2
0
-2
-4
Aox3
Gstz1
Fah
Aoc3
Adh1
C
Hif1a signalling
logFC
4
2
0
-2
-4
Gapdh
Egf
Eif4e
Tf
D
Ribosome
logFC
4
2
0
-2
-4
Rpsa
Rpl29
Rps21
Rplp0
Rps28
Rpl27
Rpl18a
Rpl38
Rpl3
LOC100362830
Rpl35
Rps17
Rps3a
Rps27l
LOC103690821
LOC108350501
Rpl7a
Rps25
Rpl12
Rpl36
Rpl6
Rpl10a
Rpl18
Rpl32
Rpl17
LOC100360522
Rpl11

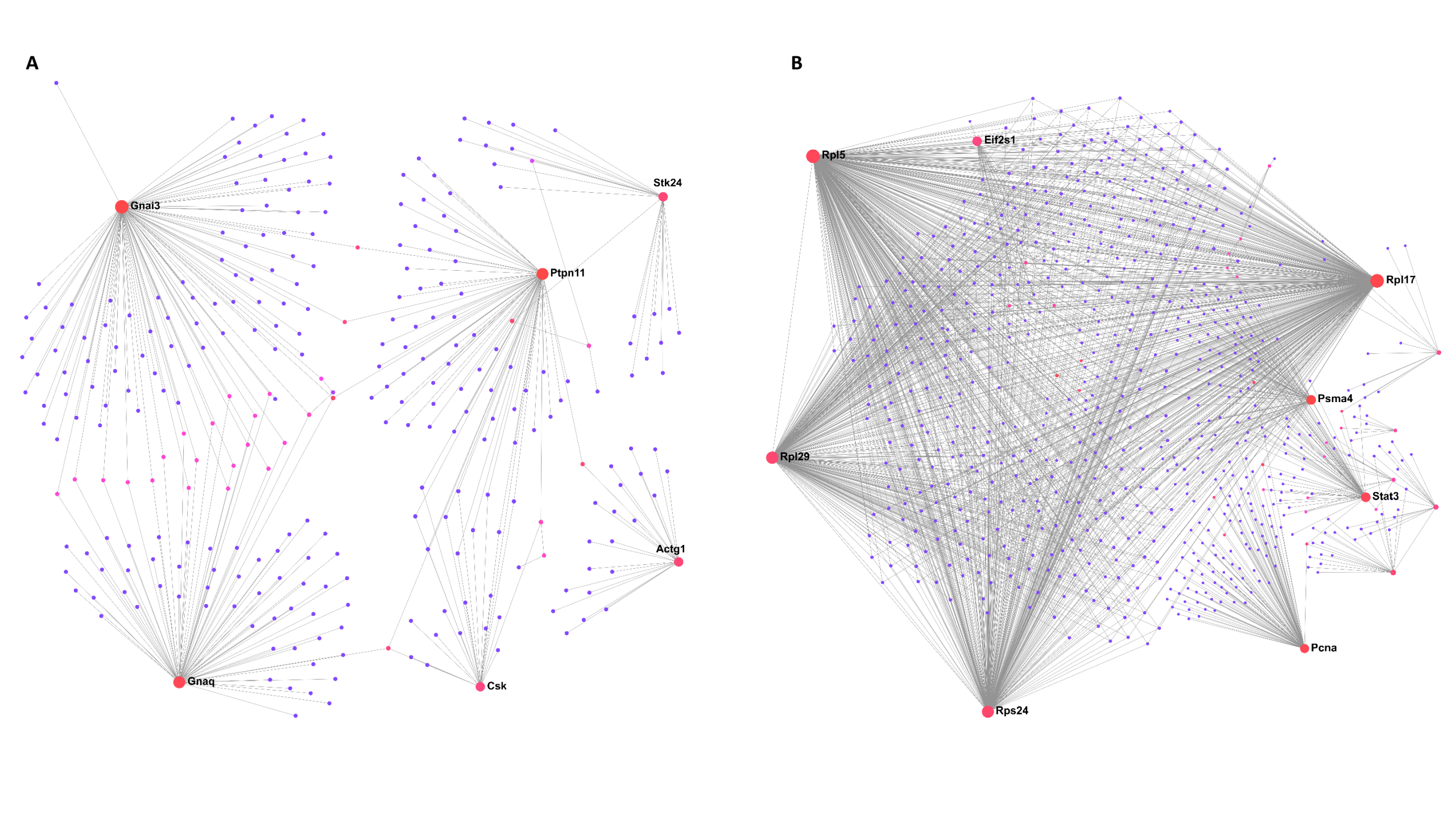
A
Gnai3
Stk24
Ptpn11
Actg1
Gnaq
Csk
B
Eif2s1
Rpl5
Rpl17
Psma4
Rpl29
Stat3
Pcna
Rps24

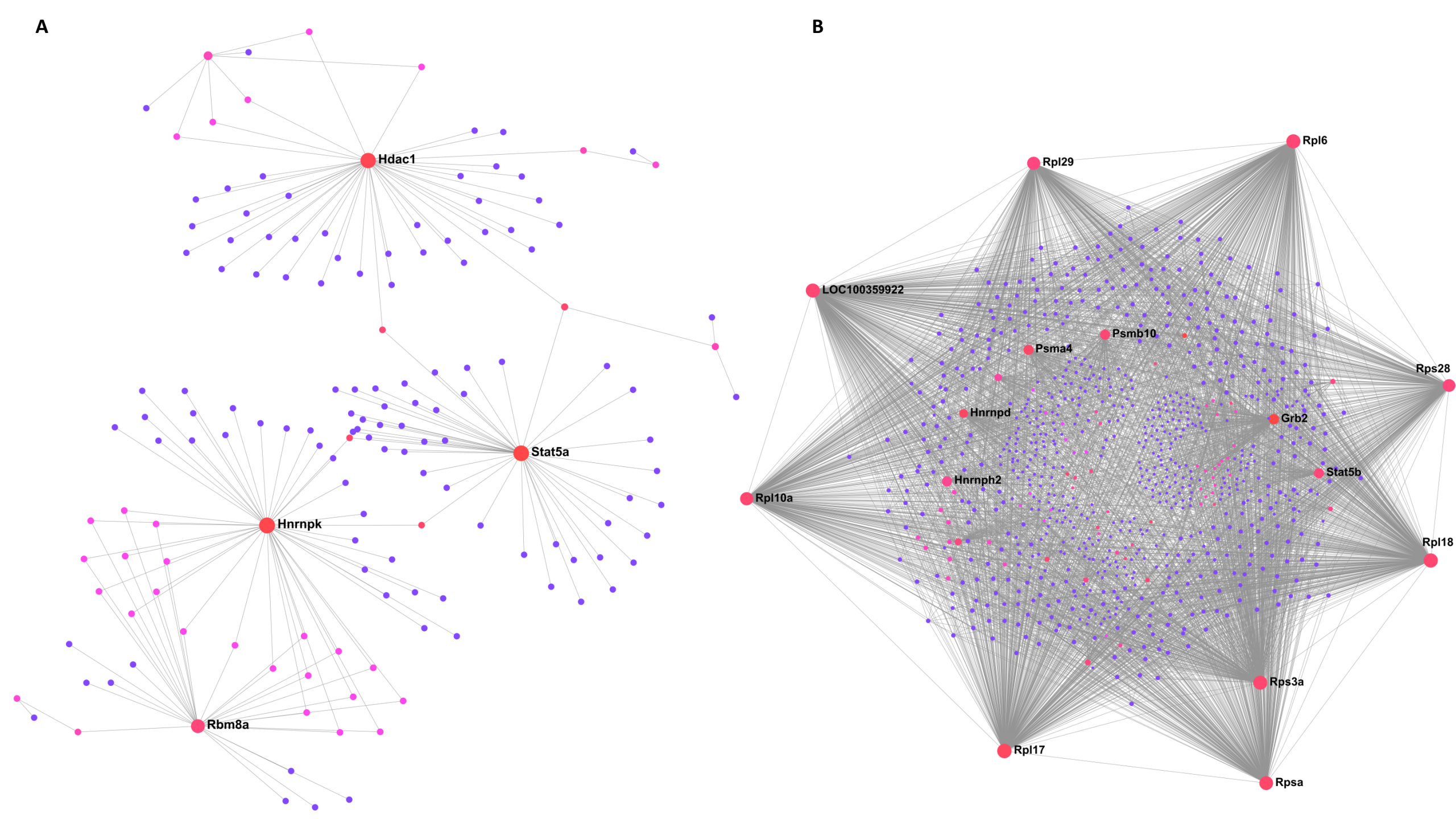
A
Hdac1
Stat5a
Hnrnpk
Rbm8a
B
Rpl6
Rpl29
LOC100359922
Psmb10
Psma4
Rps28
Hnrnpd
Grb2
Stat5b
Hnrnph2
Rpl10a
Rpl18
Rps3a
Rpl17
Rpsa